Redox Signaling in Chloroplasts: Cleavage of Disulfides by an Iron-Sulfur Cluster

Shaodong Dai,[1]* Cristina Schwendtmayer,[2] Peter Schürmann,[2]
S. Ramaswamy,[1]† Hans Eklund[1]‡

Light generates reducing equivalents in chloroplasts that are used not only for carbon reduction, but also for the regulation of the activity of chloroplast enzymes by reduction of regulatory disulfides via the ferredoxin:thioredoxin reductase (FTR) system. FTR, the key electron/thiol transducer enzyme in this pathway, is unique in that it can reduce disulfides by an iron-sulfur cluster, a property that is explained by the tight contact of its active-site disulfide and the iron-sulfur center. The thin, flat FTR molecule makes the two-electron reduction possible by forming on one side a mixed disulfide with thioredoxin and by providing on the opposite side access to ferredoxin for delivering electrons.

Redox signaling and regulation has become an area of increasing interest given that transcription, translation, apoptosis, and enzymatic activity can be regulated in this way (*1*). This type of regulation was first described for the activation of chloroplast enzymes by light through the reduction of disulfides, thereby changing the metabolism to become anabolic (*2*). Thioredoxins are the key transmitters of reducing equivalents to target enzymes.

The photosynthetic machinery in plants and other photosynthetic organisms produces reducing equivalents; e.g., nicotinamide adenine dinucleotide phosphate, reduced (NADPH), in the light reactions that together with the generated adenosine 5′-triphosphate are necessary to reduce CO_2 to carbohydrates (*2*). Plants satisfy their energy needs through the light reactions of photosynthesis during light periods. The situation is quite different in the dark, when the plant must use normal catabolic processes as do nonphotosynthetic organisms. The stroma in the chloroplasts contains both assimilatory enzymes of the Calvin cycle and dissimilatory enzymes, which implies that there must be a light-sensitive control to balance these reactions.

One such regulatory mechanism senses the light-dependent redox potential changes of the stroma and translates them into signals that, in the light, stimulate the Calvin cycle and deactivate degradative pathways (*2*, *3*). The enzyme ferredoxin:thioredoxin reductase (FTR) is a key component of this system. During light reactions photosystem I reduces ferredoxin, which is used by $NADP^+$:ferredoxin reductase to produce NADPH for the carbon reduction. The reduced ferredoxin is also used by FTR to produce reduced thioredoxins, which activate fructose-1,6-bisphosphatase, sedoheptulose-1,7-bisphosphatase, and phosphoribulokinase of the Calvin cycle as well as other chloroplast enzymes by disulfide reduction (*3*). Recently the structures of several members of this regulatory chain have been determined (Fig. 1). Here we report the structure of the last missing member of the chain, FTR. This enzyme is the central actor that transforms the electron signal received from ferredoxin to a thiol signal that is transmitted to thioredoxin. The results provide the structural framework for this mechanism.

FTR is a unique enzyme, completely different from the bacterial and mammalian thioredoxin reductases, which are flavoproteins that use NADPH as reductant. FTR is an iron-sulfur enzyme, an $\alpha\beta$ heterodimer composed of a catalytic β subunit of 13 kD with conserved sequence between species and a variable α subunit of similar size. The β subunit contains a redox-active disulfide and a [4Fe-4S] center. Most biochemical investigations have been done on the spinach enzyme, for which a careful study of the iron-sulfur center has been performed (*4*). We have determined the structure of FTR from *Synechocystis* sp. PCC6803. The *Synechocystis* FTR shows no functional difference from the spinach enzyme, but it is significantly more stable and can be obtained in larger amounts (*5*). The structure of the oxidized FTR was determined by multiple isomorphous replacement (MIR) with the help of multiwavelength anomalous dispersion (MAD) data collected on the iron edge for the iron-sulfur center. The structure has been refined at 1.6 Å resolution (*6*).

The variable chain in FTR has an open β-barrel structure containing five antiparallel strands (Fig. 2A). Two loops between the β strands dominate the interaction area with the catalytic subunit. The structure of the variable chain of FTR is remarkably similar to

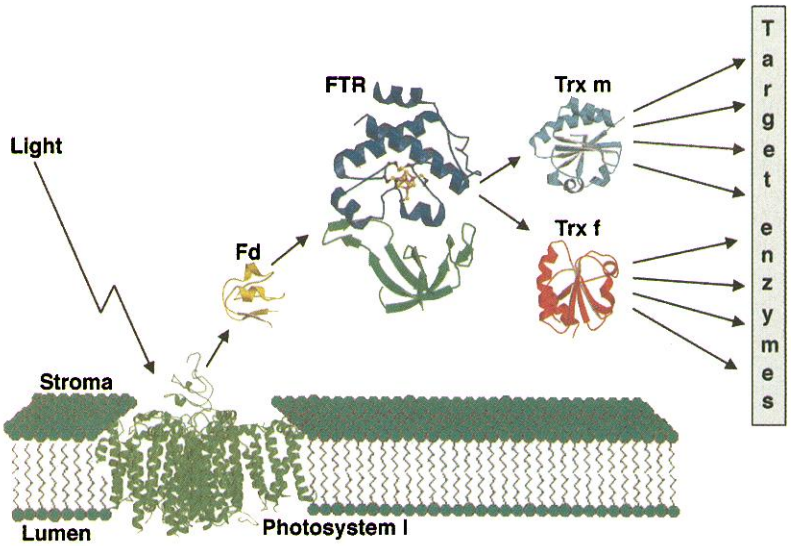

Fig. 1. FTR has a key position in light-induced enzyme regulation in chloroplasts. Upon illumination, the photosynthetic electron transfer chain reduces ferredoxin (Fd) (*25*) by photosystem I (*8*). Ferredoxin can then reduce ferredoxin:thioredoxin reductase (FTR), which reduces the chloroplast thioredoxins m and f (Trx m and Trx f) (*26*). Finally, the thioredoxins activate (in some cases deactivate) target enzymes, thereby switching the metabolism to anabolic pathways. Arrows indicate the flow of electrons. The molecular basis for light activation of the target enzyme malate dehydrogenase from C_4-plants has recently been revealed from crystal structures (*27*).

---

[1] Department of Molecular Biology, Swedish University of Agricultural Sciences, Box 590, Biomedical Center, S-751 24 Uppsala, Sweden. [2] Laboratoire de Biochimie Végétale, Université de Neuchâtel, CH-2007 Neuchâtel, Switzerland.

*Present address: Department of Biological Sciences, 1392 Lilly Hall of Life Sciences, Purdue University, West Lafayette, IN 47907, USA.

†Present address: Department of Biochemistry, University of Iowa, 51 Newton Road, Iowa City, IA 52242–1109, USA.

‡To whom correspondence should be addressed. E-mail: hasse@xray.bmc.uu.se

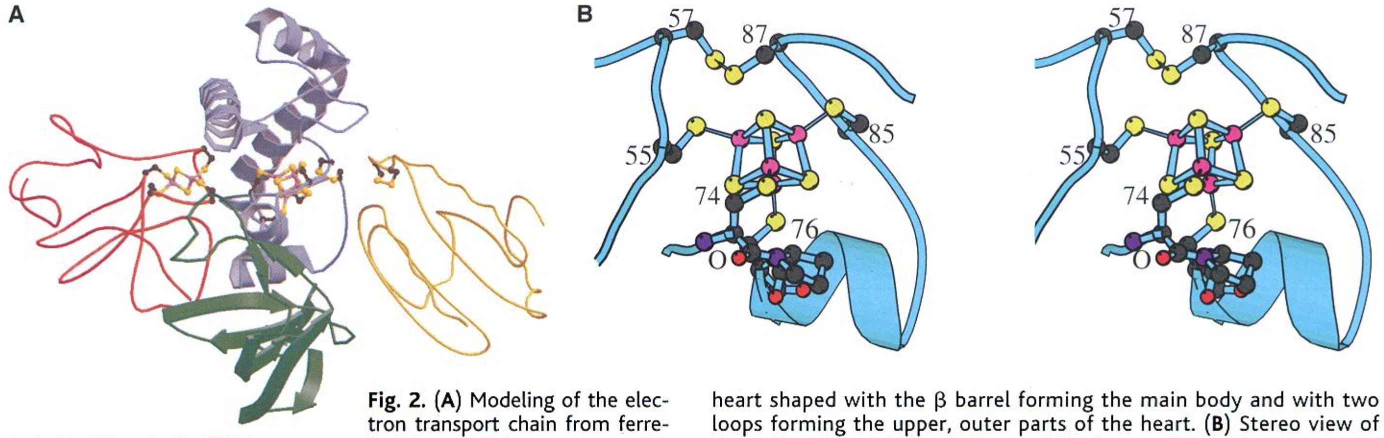

Fig. 2. (**A**) Modeling of the electron transport chain from ferredoxin to thioredoxin. FTR is an unusually thin molecule, a concave disk with dimensions 40 Å by 50 Å but only 10 Å across the center of the molecule where the iron-sulfur cluster is located. The disk-shaped structure of the FTR allows docking of a ferredoxin on one side of the molecule (red, to the left), while thioredoxin binds to the other side and forms a heterodisulfide with the enzyme (yellow, to the right). This intermediate can be reduced by an electron from a second ferredoxin molecule. The iron-sulfur centers and disulfide bridges are shown in ball-and-stick representation. The catalytic subunit of FTR (blue) has an overall α-helical structure with loops between the helices containing the iron-sulfur ligands and redox-active cysteines. The variable subunit (green) is heart shaped with the β barrel forming the main body and with two loops forming the upper, outer parts of the heart. (**B**) Stereo view of the active site of FTR. The irons of the iron-sulfur center are coordinated by cysteines 55, 74, 76, and 85 in a normal cubane-type geometry. The active-site disulfide bridge between residues 57 and 87 is in van der Waals contact with the iron center. The sulfur atom of Cys^{87} contacts the iron atom bound by Cys^{55} and the sulfur atom of Cys^{55}, both of which are at 3.1 Å distance. The closest sulfide ion of the cluster is 3.5 Å away from Cys^{87}. Besides the active-site cysteines, Pro^{75} is also shown in ball-and-stick models. Incoming electrons can pass from ferredoxin onto the main chain of Cys^{74} to the disulfide bridge by way of the iron center. The oxygen atom in the *cis*-peptide bond between Cys^{74} and Pro^{75} is labeled.

that of the PsaE protein, which is a stromal subunit of photosystem I (*7*, *8*). Two-thirds of the variable chain (53 Cα atoms of the two proteins) can be superimposed with a root-mean-square (rms) fit of 1.3 Å. The strands of the barrel are very similar in the two structures, while the loops differ. The similarities of the variable subunit of FTR and PsaE are not reflected in sequence similarities nor in functional similarities. The proteins have no common ferredoxin binding site, which might have been anticipated. All conserved residues in the variable chain are either internal or glycines that are conserved for structural reasons, and residues in the interaction area with the catalytic subunit.

The catalytic subunit has an overall α-helical structure with loops between the helices containing the iron-sulfur ligands and redox-active cysteines (Fig. 2A). The NH_2-terminal half of the subunit, together with the COOH-terminal residues, forms an α-helical cap on top of the iron-sulfur center, while the intervening 40 residues contain all the iron ligands and redox-active cysteines. This part contains two additional short helices and intervening loops.

The interaction between the catalytic and variable chains involves the very thin center of the molecule where only a small hydrophobic core is formed. However, most of the interactions between the subunits occur between charged and polar residues that form hydrogen bonds. Practically all residues in the catalytic subunit that participate in subunit interactions are strictly conserved. One important function of the variable subunit seems to be the stabilization of the Fe-S cluster, which might ensue from the observation that most residues involved in subunit interaction are conserved. We have seen that upon treatment of FTR with increasing concentrations of urea or guanidine-HCl, the color of the FTR disappears when the FTR dissociates into subunits. Production of only recombinant catalytic subunit yields neither colored nor active protein.

The irons of the iron-sulfur center (Fig. 2B) are coordinated by cysteines 55, 74, 76, and 85 in a normal cubane-type geometry (*9*). The sulfur atoms of the liganding cysteines are hydrogen-bonded to main chain nitrogen atoms (*10*). None of the sulfide ions have a hydrogen bond to a protein atom. The iron center is surrounded exclusively by hydrophobic residues, all coming from the catalytic subunit.

The sequence fingerprints for FTRs differ from those for other iron-sulfur proteins where the liganding cysteines are separated by at least two residues. The common binding motif for [4Fe-4S] clusters, the CXXC motif (*11*), is absent in FTR. Rather, all ligands are located in short sequence motifs CXC, which is a unique arrangement with the fingerprint $\mathbf{C}XCx_{16}\mathbf{C}X\mathbf{C}x_8\mathbf{C}XC$ (cluster ligands in bold type). Both cysteines in the central CPC motif are ligands to the iron-sulfur center. In the other two motifs, the liganding cysteines are connected to the redox-active cysteines in a CPC and a CHC motif. The latter cysteines in these motifs are forming the disulfide bridge. The active-site disulfide bridge between residues 57 and 87 is in van der Waals contact with the iron center; primarily, the sulfur atom of Cys^{87} contacts the iron atom bound by Cys^{55}. Cys^{57} is at the molecular surface and should be the nucleophile in thiol-disulfide exchange reactions during thioredoxin reduction. His^{86} is very close to the disulfide bridge and might increase the nucleophilicity of the cysteine.

In analogy to known mechanisms, the reduction of thioredoxin has been proposed to proceed by way of a mixed disulfide bond between thioredoxin and FTR (*4*). Such an intermediate complex would cover one of the sides of the flat FTR molecule, and the second electron for the reduction should be delivered by the next incoming ferredoxin, which has to dock on the opposite side of the flat, disklike heterodimer. The structure of the FTR dimer suggests that the two separate essential interaction surfaces for ferredoxin and thioredoxin involve both FTR subunits. The FTR heterodimer is an unusually thin molecule, a concave disk with only 10 Å across the center of the molecule where the iron-sulfur center is located (Fig. 2A). One side of the iron-sulfur center is covered by the redox-active disulfide that reduces thioredoxin in a thiol-disulfide exchange reaction. FTR (as PsaE) is structurally similar to the SH3 domains, and the peptide binding site of the SH3 domain corresponds in FTR to a part of the binding site for thioredoxin. The opposite side of the disk has shape complementarity to the ferredoxin molecule (*12*).

The FTR molecule seems ideally suited for electron transfer between ferredoxin and thioredoxin (Fig. 2A). The iron-sulfur ligands on the side of the disk-shaped FTR molecule that is complementary to ferredoxin are connected by Pro^{75} (the only cis-proline in the

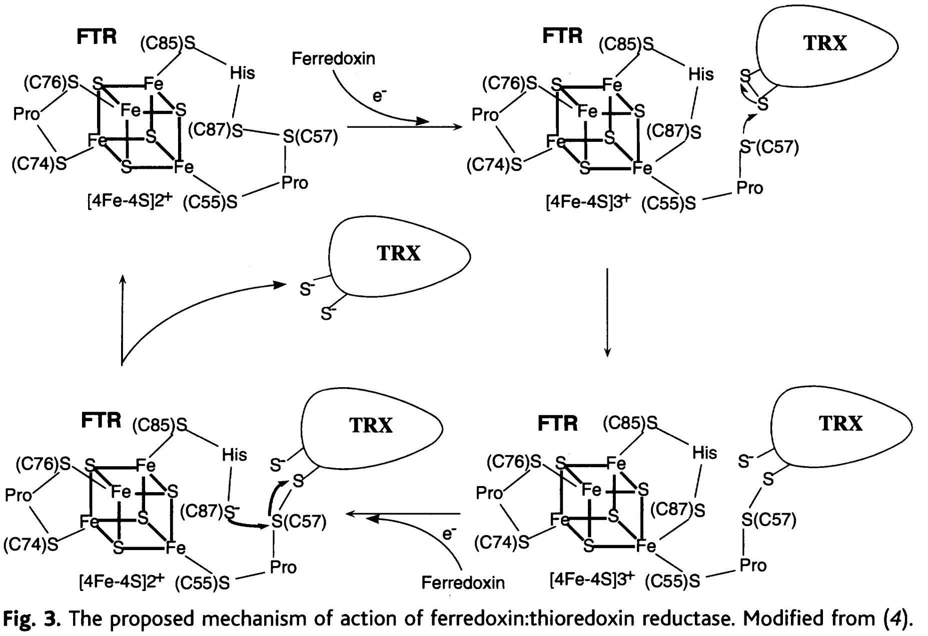

Fig. 3. The proposed mechanism of action of ferredoxin:thioredoxin reductase. Modified from (*4*).

structure) in one CPC motif. The main chain of this motif is exposed toward the ferredoxin side and provides excellent candidates for through-bond electron transfer from the bound ferredoxin to the iron-sulfur center (Fig. 2B).

All other biological disulfide reactions occur by means of flavoproteins or thiol-disulfide exchange reactions. The close proximity of iron-sulfur cluster and disulfide is evidently a prerequisite for FTR's unique property of being able to reduce the disulfide by an iron-sulfur center. The disulfide that is adjacent to one iron atom of the cluster can pick up an electron delivered by ferredoxin to the iron-sulfur cluster of FTR but it can also attract one additional electron from the iron-sulfur center to break the disulfide bond. One of the cysteines, Cys^{57}, becomes then the reactive thiol, while the second cysteine thiol is protected by binding to the iron-sulfur cluster. Therefore, the one-electron reduction of FTR by ferredoxin surprisingly results in an oxidation of the [4Fe-4S]$^{2+}$ cluster to an [4Fe-4S]$^{3+}$ cluster (*4*) (Fig. 3). Two structures for this intermediate stage have been suggested: with Cys^{87} covalently attached to the cluster either through an Fe atom or a sulfide ion (*4*). Staples *et al.* (*4*) favor an intermediate disulfide of Cys^{87} with the sulfide ion. The tight interaction by Cys^{87} with one of the irons of the cluster in the FTR structure instead implicates that Cys^{87} coordinates the iron in a five-coordinated cluster (Fig. 3). Although there is no example to our knowledge of a cysteine-sulfide bridge in an iron-sulfur cluster, there is some precedence for this type of pentacoordinated iron given that five-coordinated subsites of [4Fe-4S] clusters have been synthesized (*13*). Higher coordination of iron in iron-sulfur clusters occurs also for aconitase-substrate complexes (*14*). Furthermore, five-coordinated iron clusters show modified redox potentials (*13*) analogous to those found for FTR (*4*). For the FTR intermediate, the redox potential of the [4Fe-4S]$^{3+,2+}$ couple is lowered from +420 to −210 mV, which is in the same region as the redox potential for the active-site disulfide (*4*, *5*, *15*). A similar lowering of redox potential by about 300 to 700 mV is observed for five-coordinated iron clusters compared with four-coordinated iron clusters (*13*).

The one-electron reduced intermediate, with its nucleophilic thiol Cys^{57}, is able to attack the disulfide bridge of thioredoxin to form a hetero-disulfide. The next electron delivered by a new ferredoxin molecule reduces the iron-sulfur center back to its original oxidation state, thereby reducing the disulfide bridge between FTR and thioredoxin and releasing the fully reduced thioredoxin. Such a mechanism, which requires the simultaneous docking of thioredoxin and ferredoxin, is entirely compatible with the disk-shaped structure of FTR, which would allow docking of a second ferredoxin on one side of the molecule, while thioredoxin is bound to the other side by way of the intermolecular disulfide bridge (Fig. 2A).

Note added in proof: Recently, the structure of the redox-regulated target enzyme fructose-1,6-bisphosphate phosphatase was published (*28*).

References and Notes

1. C. Abate, L. Patel, F. J. Raucher, T. Currran, *Science* **249**, 1157 (1990); S. Xanthoudakis, G. G. Miao, T. Curran, *Proc. Natl. Acad. Sci. U.S.A.* **91**, 23 (1994); J. Qin, G. M. Clore, W. M. Kennedy, J. R. Huth, A. M. Gronenborn, *Structure* **3**, 289 (1995); J. Qin, G. M. Clore, W. P. Kennedy, J. Kuszewski, A. M. Gronenborn, *Structure* **4**, 613 (1996); M. B. Hampton and S. Orrenius, *Biofactors* **8**, 1 (1998); C. K. Sen, *Biochem. Pharmacol.* **55**, 1747 (1998); A. Danon and S. P. Mayfield, *Science* **266**, 1717 (1994); C. S. Levings III and J. N. Siedow, *Science* **268**, 695 (1995).
2. B. B. Buchanan, *Annu. Rev. Plant Physiol.* **31**, 341 (1980); *Arch. Biochem. Biophys.* **288**, 1 (1991); ———, P. Schürmann, P. Decottignies, R. M. Lozano, *Arch. Biochem. Biophys.* **314**, 257 (1994).
3. J.-P. Jacquot, J.-M. Lancelin, Y. Meyer, *New Phytol.* **136**, 543 (1997).
4. C. R. Staples *et al.*, *Biochemistry* **35**, 11425 (1996); C. R. Staples *et al.*, *Biochemistry* **37**, 4612 (1998).
5. C. Schwendtmayer, W. Manieri, M. Hirasawa, D. B. Knaff, P. Schürmann, *Proceedings of the XIth International Congress on Photosynthesis*, Budapest, Hungary, 17 to 22 August 1998, G. Garab, Ed. (Kluwer, Dordrecht, Netherlands, 1998), vol. 3, pp. 1927–1930.
6. Crystals were obtained by hanging drop vapor diffusion with equal volumes of concentrated protein (17 mg/ml) containing 20 mM triethanolamine-HCl (pH 7.3) and reservoir solution containing 2.0 M ammonium sulfate, 0.1 M NaAc (pH 5.1), and 100 mM MgCl$_2$. These crystals belong to space group $P4_32_12$ with cell constants $a = b = 45.2$ Å and $c = 172.6$ Å. MAD data at three wavelengths on the iron edge were collected on beamline BM14 at the European Synchrotron Radiation Facility, Grenoble, France. The images were processed with DENZO (*16*) and merged and scaled with AGROVATA from CCP4 programs (*17*). EMTS, UO$_2$Ac$_2$, and KAu(CN)$_2$ derivative data were collected at BL-711, MAXII lab in Lund, Sweden. A 1.6 Å native data set was collected at the BW7B beamline at the European Molecular Biology Laboratory, Desy, Hamburg. The R_{sym} was 0.05 for all data and 0.20 for the highest resolution shell (1.7 to 1.6 Å). The corresponding redundancy was 3.0 and 2.6, respectively. The four Fe sites and heavy-atom sites from three derivatives were refined together in SHARP (*18*) and MLPHARE (*19*). The initial MIR phases could be improved by solvent flattening, histogram matching, and skeletonization in DM (*20*). Models were constructed in program O (*21*). The FTR structure was refined with REFMAC (*22*) at 1.6 Å resolution. Waters were added with the program ARP (*23*). The well-ordered protein atoms and the [4Fe-4S] cluster have been refined with restrained individual isotropic temperature factors. One hundred and forty-seven water molecules and one sulfate ion have been added. The R value for all reflections in the resolution range 15 to 1.6 Å is 23% (R_{free} of 28%). Ninety-two percent of all residues are in the most favorable area and there are no residues in generously allowed or disallowed regions (*24*). One *cis*-proline (Pro^{75}) is located between the Cys^{74} and Cys^{76} that are liganded to the [4Fe-4S] cluster.
7. C. J. Falzone, H. Kao, J. Zhao, D. A. Bryant, J. T. Lecomte, *Biochemistry* **33**, 6052 (1994); K. L. Mayer, G. Shen, D. A. Bryant, J. T. Lecomte, C. J. Falzone, *Biochemistry* **38**, 13736 (1999).
8. W. D. Schubert *et al.*, *J. Mol. Biol.* **280**, 297 (1998); O. Klukas *et al.*, *J. Biol. Chem.* **274**, 7351 (1999); J. J. van Thor, T. H. Geerlings, H. C. P. Matthijs, K. J. Hellingwerf, *Biochemistry* **38**, 12735 (1999).
9. H. Beinert, R. H. Holm, E. Münck, *Science* **277**, 653 (1997); C. D. Stout, E. A. Stura, D. E. McRee, *J. Mol. Biol.* **278**, 629 (1998). The positions of the atoms in the cluster deviate by an rms of 0.05 Å from the atoms of the superimposed [4Fe-4S] cluster of *Azotobacter vinelandii* ferredoxin (Protein Data Bank accession code 6fd1).
10. E. Adman, K. D. Watenpaugh, L. H. Jensen, *Proc. Natl. Acad. Sci. U.S.A.* **72**, 4854 (1975); G. Backes *et al.*, *J. Am.Chem. Soc.* **113**, 2055 (1991); R. Langen, G. M. Jensen, U. Jacob, P. J. Stephens, A. Warshel, *J. Biol. Chem.* **267**, 25625 (1992).
11. J. B. Howard and D. C. Rees, *Adv. Protein Chem.* **42**, 199 (1991).
12. The surfaces on both sides of the molecule are highly conserved. The potential ferredoxin interaction area contains three positively charged residues at about 10 Å from the cluster. Together with hydrophobic residues around the Fe-S cluster they form a docking area for the negatively charged ferredoxin. The thioredoxin interaction area is different and contains more hydrophobic residues and three histidines, one

of them very close to the active site. There is one negatively charged residue, Glu^{84}, about 12 Å away from the FTR disulfide, which fits with a positively charged residue in thioredoxin. The absence of charged groups, except for the one, makes the thioredoxin interaction area less specific, which might be important because FTR reduces different thioredoxins present in the cell, as is the case in the spinach chloroplast. Even *Synechocystis* FTR is capable of reducing spinach thioredoxin f. The ferredoxin interaction area, by contrast, is more specific owing to the presence of several charged residues. We observed a lower affinity between spinach ferredoxin and *Synechocystis* FTR (*5*) than was reported for the homologous couple spinach ferredoxin and FTR [M. Hirasawa *et al.*, *Biochim. Biophys. Acta* **935**, 1 (1988)].

13. S. Ciurli *et al.*, *J. Am. Chem. Soc.* **112**, 2654 (1990).
14. H. Laube, M. C. Kennedy, H. Beinert, C. D. Stout, *J. Mol. Biol.* **237**, 437 (1994).
15. M. Hirasawa *et al.*, *Biochemistry* **38**, 5200 (1999); Z. Salamon *et al.*, *Biochem. Biophys. Acta* **1230**, 114 (1995).
16. Z. Otwinowski and W. Minor, *Methods Enzymol.* **276**, 307 (1997).
17. D. Bailey, *Acta Crystallogr.* **D50**, 760 (1994).
18. E. de La Fortelle and G. Bricogne, *Macromol. Crystallogr.* **276**, 442 (1997).
19. Z. Otwinowski, in *Proceedings of the CCP4 Study Weekend*, W. Wolf, P. R. Evans, A. G. W. Leslie, Eds. (Science and Engineering Research Council, Daresbury Laboratory, Warrington, UK, 1991), pp. 80–88.
20. K. Cowtan, *Joint CCP4 ESF-EACBM Newslett. Protein Crystallogr.* **31**, 34 (1994).
21. T. A. Jones, J. Y. Zou, S. W. Cowan, M. Kjeldgaard, *Acta Crystallogr.* **47**, 110 (1991).
22. G. N. Murshudov, A. A. Vagin, E. J. Dodson, *Acta Crystallogr.* **D53**, 240 (1997).
23. V. S. Lamzin and K. S. Wilson, *Acta Crystallogr.* **D49**, 129 (1993).
24. R. A. Laskowski, M. W. MacArthur, D. S. Moss, J. M. Thornton, *J. Appl. Crystallogr.* **26**, 283 (1993).
25. B. L. Jacobson, Y. K. Chae, J. L. Markley, I. Rayment, H. M. Holden, *Biochemistry* **32**, 6788 (1993).
26. G. Capitani *et al.*, in (*5*), pp. 1939–1942.
27. K. Johansson *et al.*, *Biochemistry* **38**, 4319 (1999); P. D. Carr, D. Verger, A. R. Ashton, D. L. Ollis, *Structure* **7**, 461 (1999).
28. M. Chiadmi, A. Navazo, M. Miginac-Maslow, J.-P. Jacquot, J. Cherfils, *EMBO J.* **18**, 6809 (1999).

29. Supported by grants from the Swedish Council for Forestry and Agricultural Research and Swedish Natural Science Research Council (to H.E) and the Schweizerischer Nationalfonds (31-47107.96 to P.S.). Coordinates have been deposited in the Protein Data Bank (accession code 1dj7).

18 October 1999; accepted 7 December 1999

Voltage- and Tension-Dependent Lipid Mobility in the Outer Hair Cell Plasma Membrane

John S. Oghalai, Hong-Bo Zhao, J. Walter Kutz, William E. Brownell*

The mechanism responsible for electromotility of outer hair cells in the ear is unknown but is thought to reside within the plasma membrane. Lipid lateral diffusion in the outer hair cell plasma membrane is a sigmoidal function of transmembrane potential and bathing media osmolality. Cell depolarization or hyposmotic challenge shorten the cell and reduce membrane fluidity by half. Changing the membrane tension with amphipathic drugs results in similar reductions. These dynamic changes in membrane fluidity represent the modulation of membrane tension by lipid-protein interactions. The voltage dependence may be associated with the force-generating motors that contribute to the exquisite sensitivity of mammalian hearing.

Membranes define the boundaries of cells and maintain the electrochemical gradients required for life. In addition, the lateral wall plasma membrane of the mammalian cochlear outer hair cell (OHC) is involved in voltage-dependent changes in cell length, or electromotility (*1*). OHC electromotility is fundamental to the hearing sensitivity and selectivity of all mammals (*2*), but its mechanism is not known. Voltage-dependent changes in cell length must involve interactions between components of the plasma membrane and the cytoskeleton. We sought to investigate these lipid-protein interactions by measuring the fluidity of the phospholipid bilayer under three different experimental manipulations. We varied the membrane potential, modulated the intracellular pressure, and added drugs known to change membrane tension and curvature.

The rate of lateral diffusion of intramembrane lipids provides a measure of membrane fluidity (*3*). Lipid lateral diffusion can be affected by the phase state of the membrane, the individual types of membrane components (phospholipids, cholesterol, and protein), and their interactions (*4*). Guinea pig OHCs were isolated in vitro and stained with a fluorescent membrane lipid (di-8-ANEPPS) (*5*). We measured the lateral diffusion of di-8-ANEPPS in the lateral wall plasma membrane with fluorescence recovery after photobleaching (*6*). The diffusion coefficient of the lateral wall plasma membrane measured in this study ranged between 1.34×10^{-9} and 7.16×10^{-9} cm^2/s. These values are comparable to those previously reported for the OHC and lie within the range of those reported for other eukaryotic membranes (*5*, *7*).

OHC membrane potential was controlled by voltage clamp during measures of lateral diffusion (*8*). Membrane fluidity was voltage-dependent, decreasing up to 51% with depolarization (Fig. 1A). Saturation of the diffusion coefficient occurred at the voltage extremes. Sequential measurements of the diffusion coefficient in single cells at −60 mV, 0 mV, and then again at −60 mV revealed the voltage-dependent change in lateral diffusion to be reversible. The average diffusion coefficient went from $4.26 \times 10^{-9} \pm 0.42 \times 10^{-9}$ to $1.96 \times 10^{-9} \pm 0.33 \times 10^{-9}$ to $3.74 \times 10^{-9} \pm 0.55 \times 10^{-9}$ cm^2/s (mean ± SEM; $n = 4$). The diffusion coefficient in cultured rat hippocampal neurons (our control cells) did not change with changes in holding potential, going from $3.55 \times 10^{-9} \pm 0.24 \times 10^{-9}$ cm^2/s at −60 mV to $3.59 \times 10^{-9} \pm 0.21 \times 10^{-9}$ cm^2/s at 0 mV (mean ± SEM; $n = 9$).

Changes in membrane potential result in OHC length changes. Another way to change OHC length is to vary the intracellular pressure by changing the osmolality of the extracellular bathing media (*9*). Solutions with lower osmolality caused cell shortening and a decrease in the diffusion coefficient (Fig. 1, B and C). These effects were reversible, and both the cell length and the diffusion coefficient saturated at the osmotic extremes. The relation of cell length to membrane fluidity is exponential (Fig. 1D). Deiters' cells (supporting cells in the cochlea that co-isolate with OHCs) were used as controls. They underwent shape changes in response to osmotic challenge but had no change in their membrane diffusion coefficient.

Finally, the plasma membrane was directly manipulated by applying amphipathic drugs known to change membrane tension and curvature in red blood cells (RBCs) and COS cell cultures (*10*). The bilayer-couple hypothesis (*11*) argues that drugs which alter membrane curvature preferentially partition into either the outer or the inner leaflet of the phospholipid bilayer, selectively increasing that leaflet's surface area. Differences between outer and inner leaflet area alter membrane tension and curvature. We applied a drug that bends membranes outward (salicylate) and another that bends membranes inward (chlorpromazine) to a preparation containing guinea pig OHCs and RBCs (Fig. 2) (*12*). Although we found the expected morphologic changes in RBCs, the drugs evoked no change in the microscopic appearance of the OHCs ($n = 39$). However, measurements of OHC lipid lateral diffusion did show an effect of drug application (Fig. 2F). The presence of salicylate alone or chlorprom-

---

Department of Otolaryngology and Communicative Sciences, Baylor College of Medicine, One Baylor Plaza, Houston, TX 77030, USA.

*To whom correspondence should be addressed. E-mail: brownell@bcm.tmc.edu